Downlink Throughput of Cell-Free Massive MIMO Systems Assisted by Hybrid Relay-Reflecting Intelligent Surfaces

Nhan T. Nguyen*, V.-Dinh Nguyen†, Hieu V. Nguyen†, Hien Q. Ngo‡, Symeon Chatzinotas†, and Markku Juntti*
*Centre for Wireless Communications, University of Oulu, P.O.Box 4500, FI-90014, Finland
†Interdisciplinary Centre for Security, Reliability and Trust (SnT), University of Luxembourg, L-1855 Luxembourg
‡School of Electronics, Electrical Engineering and Computer Science, Queen's University Belfast, United Kingdom
nhan.nguyen, markku.juntti@oulu.fi; dinh.nguyen, hieu.vannguyen, symeon.chatzinotas@sdsu.edu; hien.ngo@qub.ac.uk

***Abstract*—We consider in this work a cell-free (CF) massive multiple-input-multiple-output (mMIMO) system where multiple hybrid relay-reflecting intelligent surfaces (HR-RIS) are deployed to assist communication between access points and users. We first present the signal model and derive the minimum-mean-square-error estimate of the effective channels. We then present a comprehensive analysis for the considered HR-RIS-aided CF mMIMO system, where the closed-form expression of the downlink throughput is derived. The presented analytical results are also valid for conventional CF mMIMO systems, i.e., CF mMIMO systems with and without passive reconfigurable intelligent surfaces. Finally, the analytical derivations are verified by extensive numerical results.**

***Index Terms*—Cell-free massive MIMO, channel estimation, hybrid relay-reflecting intelligent surface**

I. Introduction

Recently, several new network architectures and technologies have been introduced to meet the demand for extremly high spectral efficiency and low-latency wireless communications. Among them, cell-free (CF) massive multiple-input-multiple-output (mMIMO) technology can provide uniform quality-of-service (QoS) to all users in the network with simple signal processing [1]. On the other hand, a hybrid relay-reflecting intelligent surface (HR-RIS) [2]–[4] is able to customize the physical propagation environment by reflecting radio waves in preferred directions with an additional relaying gain compared to conventional passive reconfigurable intelligent surfaces (RISs). Therefore, HR-RIS-assisted CF mMIMO systems can be a symbiotic convergence of technologies for future wireless communications.

The potential performance gains of passive RISs have been analyzed and optimized in various systems, ranging from single/multiple-input-single-output (SISO/MISO) [5], [6] to MIMO systems [7]–[9]. Besides, their applications to assist CF mMIMO systems were considered in [10]–[13]. Specifically, Zhang *et al.* in [11] examined the deployment of multiple RISs around multiple access points (APs) and user equipments (UEs) to enhance the energy efficiency (EE) of the CF mMIMO system. It is shown that EE performance is improved with the deployment of a few small-to-moderate-sized RISs. In contrast, it can be significantly degraded when numerous and/or large-sized RISs are used due to the increase in RIS hardware static power consumption [11]. In [12], Huang *et al.* proposed a fully decentralized design framework for cooperative beamforming in RIS-aided CF MIMO networks, which provides a significant improvement in the system sum rate. In [14], Zhou *et al.* considered an achievable rate maximization for aerial RIS-aided CF mMIMO system with a focus on joint optimization of transmit beamforming at APs and reflecting coefficients at RISs. Trinh *et al.* in [13] further verified the performance improvement of RIS-aided in CF mMIMO systems under channel spatial correlation.

In the aforementioned RIS-aided cellular and CF MIMO systems, RISs only offer passive reflecting gains. In contrast, the HR-RIS architecture introduced recently in [2]–[4] can provide both active relaying and passive reflecting gains to the system. Specifically, an HR-RIS consists of only a single or few active elements and numerous passive reflecting elements, enabling a semi-passive beamforming concept to ensure a significant performance improvement [2]–[4], [15]. Motivated by this, we consider in this work a novel HR-RIS-aided CF mMIMO system where multiple HR-RISs are deployed to assist communications between APs and UEs. We first model the channel and signal models of the HR-RIS-aided CF mMIMO systems and derive the minimum-mean-square-error (MMSE) estimate of the effective channels. This channel estimate is then used to design matched filtering in the downlink. We then derive the closed-form expression of the downlink throughput of the considered system under the assumption of the Rician fading channel model. We note that conventional CF mMIMO systems with and without purely passive RISs are special cases of the considered HR-RIS-aided CF mMIMO system. Therefore, our analytical derivations are generalized as the closed-form throughput expressions of these conventional systems. According to the authors' best knowledge, the analytical results on the throughput of the passive RIS-aided CF mMIMO systems under Rician fading channels have not been provided in the literature. The analytical derivations in this work also provide a novel framework and guidance for designing new transmission strategies and optimizing the performance of RIS/HR-RIS-enabled systems.

II. HR-RIS, Channel Model, Uplink Training, and Downlink Data Transmission

We consider an HR-RIS-aided CF mMIMO system, where L APs, each equipped with $N_{\rm A}$ transmit antennas, simultaneously serve K single-antenna UEs. We assume that all APs are connected to the central processing unit (CPU) via ideal backhaul links that offer error-free and infinite capacity [1]. Furthermore, we assume the time-division duplex (TDD) operation, focusing on the uplink training and downlink payload data transmission phases. The communications between APs and UEs are aided by M HR-RISs, each is equipped with N elements, including $N_{\rm R}$ active relay elements and $N - N_{\rm R}$ passive reflecting elements. Let $\mathcal{A}_m \subset \{1, 2, \ldots, N\}$ with $|\mathcal{A}_m| = N_{\rm R}$ denote the index set of the active elements in the mth HR-RIS. Let α_{mn} be the relay/reflection coefficient of the nth element in the mth HR-RIS. We have $\alpha_{mn} = |\alpha_{mn}| e^{j\theta_{mn}}$, where $\theta_{mn} \in [0, 2\pi)$ represents the phase shift, and $|\alpha_{mn}| = 1$ for $n \notin \mathcal{A}_m$ [6]. Let $\boldsymbol{\Upsilon}_m = \mathrm{diag}\{\alpha_{m1}, \ldots, \alpha_{mN}\} \in \mathbb{C}^{N\times N}$ be the diagonal matrix of the coefficients of the mth HR-RIS. Furthermore, we define two diagonal matrices $\boldsymbol{\Psi}_m$ and $\boldsymbol{\Phi}_m$ such that $\boldsymbol{\Upsilon}_m = \boldsymbol{\Psi}_m + \boldsymbol{\Phi}_m$, where $\boldsymbol{\Psi}_m$ and $\boldsymbol{\Phi}_m$ contain only active relaying and passive reflecting coefficients of the mth HR-RIS, respectively. Clearly, HR-RIS becomes a conventional passive RIS if $\mathcal{A}_m = \emptyset, \forall m$. We note that the energy consumption of the HR-RIS is higher than that of the conventional passive RIS (please refer to [3] for detailed comparisons). Therefore, we are interested in the case that only a few active elements are employed, i.e., $N_{\rm R} \ll N$.

A. Channel Model

Denote by $\boldsymbol{h}_{lk}^{\rm UA} \in \mathbb{C}^{N_{\rm A}\times 1}$, $\boldsymbol{h}_{km}^{\rm US} \in \mathbb{C}^{N\times 1}$, and $\boldsymbol{H}_{lm}^{\rm SA} \in \mathbb{C}^{N_{\rm A}\times N}$ the uplink channels from the kth UE to the lth AP, from the kth UE to the mth HR-RIS, and from the mth HR-RIS to the lth AP, respectively. We consider the Rician fading model for these channels with Rician factors $\left\{\kappa_{lk}^{\rm UA}, \kappa_{km}^{\rm US}, \kappa_{lm}^{\rm SA}\right\}$ and large-scale fading coefficients $\{\zeta_{lk}^{\rm UA}, \zeta_{km}^{\rm US}, \zeta_{lm}^{\rm SA}\}$, respectively. Let $\{h_{lkt}^{\rm UA}, h_{kmn}^{\rm US}, h_{lmnt}^{\rm SA}\}$ be the tth element of $\boldsymbol{h}_{lkm}^{\rm UA}$, the nth element of $\boldsymbol{h}_{km}^{\rm US}$, and the entry on the tth row and nth column of $\boldsymbol{H}_{lm}^{\rm SA}$, respectively, $t = 1, \ldots, N_{\rm A}$, $n = 1, \ldots, N$. Let $\{\bar{h}_{lkt}^{\rm UA}, \bar{h}_{kmn}^{\rm US}, \bar{h}_{lmnt}^{\rm SA}\}$ and $\{\tilde{h}_{lkt}^{\rm UA}, \tilde{h}_{kmn}^{\rm US}, \tilde{h}_{lmnt}^{\rm SA}\}$ denote the line-of-sight (LoS) and non-LoS (NLoS) components of $\{h_{lkt}^{\rm UA}, h_{kmn}^{\rm US}, h_{lmnt}^{\rm SA}\}$, respectively. The former components are modeled as deterministic channels with unit amplitudes, while the latter components are assumed to follow the Rayleigh fading model [6], [7]. Then, we have $\left|\bar{h}_{lkt}^{\rm UA}\right| = \left|\bar{h}_{kmn}^{\rm US}\right| = \left|\bar{h}_{lmnt}^{\rm SA}\right| = 1$ and $\{\tilde{h}_{lkt}^{\rm UA}, \tilde{h}_{kmn}^{\rm US}, \tilde{h}_{lmnt}^{\rm SA}\} \sim \mathcal{CN}(0, 1)$.

Let us denote $\mu_{lkt}^{\rm UA} \triangleq \sqrt{\zeta_{lk}^{\rm UA}}\sqrt{\frac{\kappa_{lk}^{\rm UA}}{\kappa_{lk}^{\rm UA}+1}}\bar{h}_{lkt}^{\rm UA}$, $\mu_{kmn}^{\rm US} \triangleq \sqrt{\zeta_{km}^{\rm US}}\sqrt{\frac{\kappa_{km}^{\rm US}}{\kappa_{km}^{\rm UA}+1}}\bar{h}_{kmn}^{\rm US}$, $\mu_{lmnt}^{\rm SA} \triangleq \sqrt{\zeta_{lm}^{\rm SA}}\sqrt{\frac{\kappa_{lm}^{\rm SA}}{\kappa_{lm}^{\rm SA}+1}}\bar{h}_{lmnt}^{\rm SA}$, $\beta_{lk}^{\rm UA} \triangleq \frac{\zeta_{lk}^{\rm UA}}{\kappa_{lk}^{\rm UA}+1}$, $\beta_{km}^{\rm US} \triangleq \frac{\zeta_{km}^{\rm US}}{\kappa_{km}^{\rm US}+1}$, and $\beta_{lm}^{\rm SA} \triangleq \frac{\zeta_{lm}^{\rm SA}}{\kappa_{lm}^{\rm SA}+1}$. Then, the channel coefficients can be modeled as $h_{lkt}^{\rm UA} = \mu_{lkt}^{\rm UA} + \sqrt{\beta_{lk}^{\rm UA}}\tilde{h}_{lkt}^{\rm UA}$, $h_{kmnt}^{\rm US} = \mu_{kmnt}^{\rm US} + \sqrt{\beta_{km}^{\rm US}}\tilde{h}_{kmnt}^{\rm US}$, and $h_{lmnt}^{\rm SA} = \mu_{lmnt}^{\rm SA} + \sqrt{\beta_{lm}^{\rm SA}}\tilde{h}_{lmnt}^{\rm SA}$. Let $\boldsymbol{h}_{lmn}^{\rm SA}$ be the nth column of $\boldsymbol{H}_{lm}^{\rm SA}$. The effective channel between the kth UE and the lth AP can be expressed as

$$\begin{aligned}\boldsymbol{g}_{lk} &\triangleq \boldsymbol{h}_{lk}^{\rm UA} + \sum\nolimits_{m=1}^{M}\boldsymbol{H}_{lm}^{\rm SA}\boldsymbol{\Upsilon}_m\boldsymbol{h}_{km}^{\rm US}\\ &= \boldsymbol{h}_{lk}^{\rm UA} + \sum\nolimits_{m=1}^{M}\sum\nolimits_{n=1}^{N}\alpha_{mn}\boldsymbol{h}_{lmn}^{\rm SA}h_{kmn}^{\rm US}, \end{aligned} \tag{1}$$

where the last equality follows the diagonal structure of $\boldsymbol{\Upsilon}_m$.

B. Uplink Channel Estimation

In the uplink training phase, all UEs send their pilot sequences to APs for channel estimation. Let $\sqrt{\tau_{\rm p}}\boldsymbol{\varphi}_k$ be the pilot sequence of the kth UE, $\|\boldsymbol{\varphi}_k\|^2 = 1, \forall k$. Here, $\tau_{\rm p}$ is the length of $\boldsymbol{\varphi}_k$, $\tau_{\rm p} < \tau_{\rm c}$ with $\tau_{\rm c}$ denoting the coherence interval. To facilitate the analysis, we assume that the pilot sequences are mutually orthogonal, i.e., $\boldsymbol{\varphi}_k^H\boldsymbol{\varphi}_{k'} = 0$ if $k \neq k'$.

Let $\boldsymbol{Y}_l^{\rm UA}$ and $\boldsymbol{Y}_l^{\rm USA}$ denote the received pilot signals through the direct UE-AP channel and through HR-RISs, respectively. Since the HR-RISs consist of active relay elements, they amplify not only the incident signals but also the noise and self-interference (SI). As a result, the lth AP receives not only pilot signals but also SI $\boldsymbol{Z}_{{\rm SI},m} \in \mathbb{C}^{N\times\tau_{\rm p}}$, and noise $\boldsymbol{Z}_{{\rm N},m} \in \mathbb{C}^{N\times\tau_{\rm p}}$. Denote by $\boldsymbol{z}_{{\rm SI},mn}^H$ and $\boldsymbol{z}_{{\rm N},mn}^H$ the nth row of $\boldsymbol{Z}_{{\rm N},m}$ and $\boldsymbol{Z}_{{\rm SI},m}$, respectively. We adopt the SI model in [16] and assume that $\boldsymbol{z}_{{\rm SI},mn}^H \sim \mathcal{CN}(\mathbf{0}, \sigma_{\rm SI}^2\mathbf{I}_{N_{\rm A}})$ and $\boldsymbol{z}_{{\rm N},mn}^H \sim \mathcal{CN}(\mathbf{0}, \sigma_{\rm N}^2\mathbf{I}_{N_{\rm A}})$, for $n \in \mathcal{A}_m$; otherwise, they are vectors of zeros because the nth element ($n \notin \mathcal{A}_m$) of the mth HR-RIS only reflects the incident pilot signals passively [17]. Let $\rho_{\rm p}$ be the power of each UE to transmit the pilot signal. Then, $\boldsymbol{Y}_l^{\rm UA}$ and $\boldsymbol{Y}_l^{\rm USA}$ are given as

$$\boldsymbol{Y}_l^{\rm UA} = \sqrt{\tau_{\rm p}\rho_{\rm p}}\sum\nolimits_{k=1}^{K}\boldsymbol{h}_{lk}^{\rm UA}\boldsymbol{\varphi}_k^H, \tag{2}$$

$$\begin{aligned}\boldsymbol{Y}_l^{\rm USA} &= \sqrt{\tau_{\rm p}\rho_{\rm p}}\sum\nolimits_{m=1}^{M}\sum\nolimits_{k=1}^{K}\boldsymbol{H}_{lm}^{\rm SA}\boldsymbol{\Upsilon}_m\boldsymbol{h}_{km}^{\rm US}\boldsymbol{\varphi}_k^H\\ &\quad + \sum\nolimits_{m=1}^{M}\boldsymbol{H}_{lm}^{\rm SA}(\boldsymbol{\Psi}_m\boldsymbol{Z}_{{\rm SI},m} + \boldsymbol{\Psi}_m\boldsymbol{Z}_{{\rm N},m}).\end{aligned} \tag{3}$$

Let $\boldsymbol{Z}_{{\rm A},l}$ be the additive white Gaussian noise (AWGN) matrix at the lth AP, whose entries are $\mathcal{CN}(0, \sigma_{\rm N}^2)$ random variables. Then, the pilot signal received at the lth AP is given as

$$\boldsymbol{Y}_l \triangleq \boldsymbol{Y}_l^{\rm UA} + \boldsymbol{Y}_l^{\rm USA} + \boldsymbol{Z}_{{\rm A},l} = \sqrt{\tau_{\rm p}\rho_{\rm p}}\sum_{k=1}^{K}\boldsymbol{g}_{lk}\boldsymbol{\varphi}_k^H + \boldsymbol{Z}_l, \tag{4}$$

where $\boldsymbol{Z}_l \triangleq \boldsymbol{Z}_{{\rm A},l} + \sum_{m=1}^{M}\boldsymbol{H}_{lm}^{\rm SA}\boldsymbol{\Psi}_m\left(\boldsymbol{Z}_{{\rm SI},m} + \boldsymbol{Z}_{{\rm N},m}\right)$ is the aggregated noise matrix at the lth AP. Note that $\left\{\boldsymbol{Z}_{{\rm SI},m}, \boldsymbol{Z}_{{\rm N},m}, \boldsymbol{Z}_{{\rm A},l}, \boldsymbol{H}_{lm}^{\rm SA}\right\}$ are mutually independent, and in diagonal matrix $\boldsymbol{\Psi}_m$, only the diagonal entries with positions determined by $\mathcal{A}_m$ are non-zeros. Thus, the entries of $\boldsymbol{Z}_l$ have zero-mean and variance $\sigma_{{\rm p},l}^2 = \sigma_{\rm N}^2 + \sum_{m=1}^{M}\beta_{lm}^{\rm SA}\sum_{n\in\mathcal{A}_m}|\alpha_{mn}|^2\sigma_{\rm S}^2$, where $\sigma_{\rm S}^2 = \sigma_{\rm N}^2 + \sigma_{\rm SI}^2$. To estimate $\boldsymbol{g}_{lk}$, $\boldsymbol{Y}_l$ is projected onto $\boldsymbol{\varphi}_k$, yielding

$$\boldsymbol{y}_{lk} \triangleq \boldsymbol{Y}_l\boldsymbol{\varphi}_k = \sqrt{\tau_{\rm p}\rho_{\rm p}}\boldsymbol{g}_{lk} + \tilde{\boldsymbol{z}}_{lk}, \tag{5}$$

where $\tilde{\boldsymbol{z}}_{lk} = \boldsymbol{Z}_l\boldsymbol{\varphi}_k$.

Theorem 1: The MMSE estimate of $\boldsymbol{g}_{lk}$ is given by

$$\hat{\boldsymbol{g}}_{lk} = \left(\mathbf{I}_{N_{\rm A}} - \tau_{\rm p}\rho_{\rm p}\boldsymbol{C}_{lk}\boldsymbol{E}_{lk}^{-1}\right)\boldsymbol{\mu}_{lk} + \sqrt{\tau_{\rm p}\rho_{\rm p}}\boldsymbol{C}_{lk}\boldsymbol{E}_{lk}^{-1}\boldsymbol{y}_{lk}, \tag{6}$$

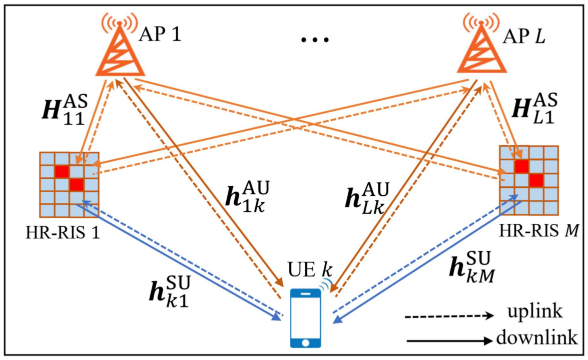

Fig. 1. Downlink channel in the HR-RIS-aided CF mMIMO system.

where

$$\boldsymbol{\mu}_{lk} = \boldsymbol{\mu}_{lk}^{\mathrm{UA}} + \sum_{m=1}^{M}\sum_{n=1}^{N} \alpha_{mn}\bar{\boldsymbol{\mu}}_{lkmn}^{\mathrm{USA}}, \tag{7}$$

$$\boldsymbol{C}_{lk} = \beta_{lk}^{\mathrm{UA}}\mathbf{I}_{N_{\mathrm{A}}} + \sum_{m=1}^{M}\sum_{n=1}^{N} |\alpha_{mn}|^2 \bar{\boldsymbol{\mathcal{B}}}_{lkmn}^{\mathrm{USA}}, \tag{8}$$

$\bar{\boldsymbol{\mu}}_{lkmn}^{\mathrm{USA}} \triangleq \boldsymbol{\mu}_{lmn}^{\mathrm{SA}}\mu_{kmn}^{\mathrm{US}}$, $\bar{\boldsymbol{\mathcal{B}}}_{lkmn}^{\mathrm{USA}} \triangleq \left(\beta_{km}^{\mathrm{US}} + \left|\mu_{kmn}^{\mathrm{US}}\right|^2\right)\beta_{lm}^{\mathrm{SA}}\mathbf{I}_{N_{\mathrm{A}}} + \beta_{km}^{\mathrm{US}}\boldsymbol{\mu}_{lmn}^{\mathrm{SA}}\left(\boldsymbol{\mu}_{lmn}^{\mathrm{SA}}\right)^H$, and $\boldsymbol{E}_{lk} \triangleq \tau_{\mathrm{p}}\rho_{\mathrm{p}}\boldsymbol{C}_{lk} + \sigma_{\mathrm{p},l}^2\mathbf{I}_{N_{\mathrm{A}}}$.

The estimate $\hat{\boldsymbol{g}}_{lk}$ has mean vector $\mathbb{E}\{\hat{\boldsymbol{g}}_{lk}\} = \boldsymbol{\mu}_{lk}$ and covariance matrix $\hat{\boldsymbol{C}}_{lk} = \tau_{\mathrm{p}}\rho_{\mathrm{p}}\boldsymbol{C}_{lk}\boldsymbol{E}_{lk}^{-H}\boldsymbol{C}_{lk}^H$, which yield

$$\mathbb{E}\left\{\hat{\boldsymbol{g}}_{lk}\hat{\boldsymbol{g}}_{lk}^H\right\} = \boldsymbol{\mu}_{lk}\boldsymbol{\mu}_{lk}^H + \hat{\boldsymbol{C}}_{lk} \triangleq \hat{\boldsymbol{R}}_{lk}, \tag{9}$$

$$\mathbb{E}\left\{\|\hat{\boldsymbol{g}}_{lk}\|^2\right\} = \|\boldsymbol{\mu}_{lk}\|^2 + \mathrm{trace}\left(\hat{\boldsymbol{C}}_{lk}\right). \tag{10}$$

The estimation error $\tilde{\boldsymbol{g}}_{lk} \triangleq \boldsymbol{g}_{lk} - \hat{\boldsymbol{g}}_{lk}$ is uncorrelated with $\hat{\boldsymbol{g}}_{lk}$ and has mean vector $\mathbb{E}\{\tilde{\boldsymbol{g}}_{lk}\} = \mathbf{0}$ and covariance matrix

$$\mathbb{C}\{\tilde{\boldsymbol{g}}_{lk}\} = \boldsymbol{C}_{lk} - \hat{\boldsymbol{C}}_{lk} \triangleq \tilde{\boldsymbol{R}}_{lk}. \tag{11}$$

Proof: Please see Appendix A. □

C. Downlink Payload Transmission

For ease of notation and due to the channel reciprocity [18], we denote the downlink channels as $\boldsymbol{h}_{lk}^{\mathrm{AU}} = (\boldsymbol{h}_{lk}^{\mathrm{UA}})^T$, $\boldsymbol{h}_{km}^{\mathrm{SU}} = (\boldsymbol{h}_{km}^{\mathrm{US}})^T$, and $\boldsymbol{H}_{lm}^{\mathrm{AS}} = (\boldsymbol{H}_{lm}^{\mathrm{SA}})^T$. Let s_k be the symbol intended for the kth UE, $\mathbb{E}\{|s_k|^2\} = 1$ and $\boldsymbol{x}_l \in \mathbb{C}^{N_{\mathrm{A}}\times 1}$ be the signal vector transmitted from the lth AP to all UEs. We assume that conjugate beamforming is employed at APs [19]. Then,

$$\boldsymbol{x}_l = \sqrt{\rho_{\mathrm{d}}}\sum\nolimits_{k=1}^{K}\sqrt{\eta_{lk}}\hat{\boldsymbol{g}}_{lk}^{*}s_k, \tag{12}$$

where ρ_{d} is the maximum transmit power at each AP, and η_{lk} is the power control coefficient for s_k. The signals propagate on the direct channels and also reflects through HR-RISs, as illustrated in Fig. 1. Therefore, the received signal at the kth UE in the downlink can be expressed as $r_k = \sum_{l=1}^{L}\boldsymbol{g}_{lk}^T\boldsymbol{x}_l + z_k$, where $z_k \triangleq \sum_{m=1}^{M}\boldsymbol{h}_{km}^{\mathrm{SU}}\boldsymbol{\Psi}_m\left(\mathrm{z}_{\mathrm{N},m} + \mathrm{z}_{\mathrm{SI},m}\right) + z_{\mathrm{U},k}$ is the aggregated noise at the kth UE, $\mathrm{z}_{\mathrm{SI},m} \sim \mathcal{CN}(\mathbf{0}, \sigma_{\mathrm{SI}}^2\mathbb{1}_m)$ is the residual SI, and $\mathrm{z}_{\mathrm{N},m} \sim \mathcal{CN}(\mathbf{0}, \sigma_{\mathrm{N}}^2\mathbb{1}_m)$ is the noise caused by active elements of the mth HR-RIS; Here, $\mathbb{1}_m$ denotes a diagonal matrix whose non-zero diagonal elements are all unity and have positions determined by $\mathcal{A}_m$; z_k has zero-mean and variance $\sigma_{\mathrm{d},k}^2 = \sigma_{\mathrm{N}}^2 + \sum_{m=1}^{M}\beta_{km}^{\mathrm{SU}}\sum_{n\in\mathcal{A}_m}|\alpha_{mn}|^2\sigma_{\mathrm{S}}^2$. Furthermore, $\boldsymbol{g}_{lk}^T = \boldsymbol{h}_{lk}^{\mathrm{AU}} + \sum_{m=1}^{M}\boldsymbol{h}_{km}^{\mathrm{SU}}\boldsymbol{\Upsilon}_m\boldsymbol{H}_{lm}^{\mathrm{AS}}$ is the effective downlink channel. From (12), r_k can be expressed as

$$r_k = \sqrt{\rho_{\mathrm{d}}}\sum_{l=1}^{L}\Big(\sqrt{\eta_{lk}}\boldsymbol{g}_{lk}^T\hat{\boldsymbol{g}}_{lk}^{*}s_k + \sum_{k'\neq k}^{K}\sqrt{\eta_{lk'}}\boldsymbol{g}_{lk}^T\hat{\boldsymbol{g}}_{lk'}^{*}s_{k'}\Big) + z_k. \tag{13}$$

III. Performance Analysis

Since there are no downlink pilot symbols, UE k treats the mean of the effective channel gain as the true channel for signal detection [1]. With this method, we rewrite (13) as

$$r_k = \mathrm{DS}_k s_k + \mathrm{BU}_k s_k + \sum_{k'\neq k}^{K}\mathrm{UI}_{kk'}s_{k'} + z_k, \tag{14}$$

where $\mathrm{DS}_k \triangleq \sqrt{\rho_{\mathrm{d}}}\mathbb{E}\left\{\sum_{l=1}^{L}\sqrt{\eta_{lk}}\boldsymbol{g}_{lk}^T\hat{\boldsymbol{g}}_{lk}^{*}\right\}$, $\mathrm{BU}_k \triangleq \sqrt{\rho_{\mathrm{d}}}\left(\sum_{l=1}^{L}\sqrt{\eta_{lk}}\boldsymbol{g}_{lk}^T\hat{\boldsymbol{g}}_{lk}^{*} - \mathbb{E}\left\{\sum_{l=1}^{L}\sqrt{\eta_{lk}}\boldsymbol{g}_{lk}^T\hat{\boldsymbol{g}}_{lk}^{*}\right\}\right)$, $\mathrm{UI}_{kk'} \triangleq \sqrt{\rho_{\mathrm{d}}}\sum_{l=1}^{L}\sqrt{\eta_{lk'}}\boldsymbol{g}_{lk}^T\hat{\boldsymbol{g}}_{lk'}^{*}$ are the desired signal, beamforming uncertainty gain, and inter-user interference, respectively. The throughput of the kth UE is given by

$$\mathcal{T}_k = \frac{B_0\tau_{\mathrm{d}}}{\tau_{\mathrm{c}}}\log_2\left(1 + \mathrm{SINR}_k\right), \tag{15}$$

where B_0 is the system bandwidth and $\tau_{\mathrm{d}} = \tau_{\mathrm{c}} - \tau_{\mathrm{p}}$ is the duration of the downlink payload transmission, and $\mathrm{SINR}_k \triangleq \frac{|\mathrm{DS}_k|^2}{\mathbb{E}\{|\mathrm{BU}_k|^2\} + \sum_{k'\neq k}^{K}\mathbb{E}\{|\mathrm{UI}_{kk'}|^2\} + \sigma_{\mathrm{d},k}^2}$.

Theorem 2: In the downlink of the considered HR-RIS-aided CF mMIMO system, the throughput of the kth UE can be approximated by (16) (at the top of the next page), where $\boldsymbol{\alpha} \triangleq \{\alpha_{mn}\}_{\forall m,n}$, $\boldsymbol{\eta} = \{\eta_{lk}\}_{\forall l,k}$, and

$$\bar{\boldsymbol{\eta}}_k \triangleq \left[\sqrt{\eta_{1k}}, \ldots, \sqrt{\eta_{Lk}}\right]^T, \tag{17}$$

$$\boldsymbol{u}_k(\boldsymbol{\alpha}) \triangleq \left[u_{1k}(\boldsymbol{\alpha}), \ldots, u_{Lk}(\boldsymbol{\alpha})\right]^T, \tag{18}$$

$$\boldsymbol{v}_{kk'}(\boldsymbol{\alpha}) \triangleq \left[v_{1kk'}(\boldsymbol{\alpha}), \ldots, v_{Lkk'}(\boldsymbol{\alpha})\right]^T, \tag{19}$$

$$\boldsymbol{D}_{kk'}(\boldsymbol{\alpha}) \triangleq \mathrm{diag}\left\{d_{1kk'}^{\frac{1}{2}}(\boldsymbol{\alpha}), \ldots, d_{Lkk'}^{\frac{1}{2}}(\boldsymbol{\alpha})\right\}. \tag{20}$$

Here, the lth elements of $\boldsymbol{u}_k(\boldsymbol{\alpha})$, $\boldsymbol{v}_{kk'}(\boldsymbol{\alpha})$, and $\boldsymbol{D}_{kk'}(\boldsymbol{\alpha})$ are defined as

$$u_{lk}(\boldsymbol{\alpha}) \triangleq \mathrm{trace}\left(\hat{\boldsymbol{C}}_{lk}\right) + \|\boldsymbol{\mu}_{lk}\|^2, \tag{21}$$

$$v_{lkk'}(\boldsymbol{\alpha}) \triangleq \boldsymbol{\mu}_{lk}^T\boldsymbol{\mu}_{lk'}^{*}, \tag{22}$$

$$d_{lkk'}(\boldsymbol{\alpha}) \triangleq \begin{cases} 2\boldsymbol{\mu}_{lk}^H\hat{\boldsymbol{C}}_{lk}\boldsymbol{\mu}_{lk} + \mathrm{trace}\left(\hat{\boldsymbol{C}}_{lk}^2 + \tilde{\boldsymbol{R}}_{lk}\circ\hat{\boldsymbol{R}}_{lk}\right), k = k' \\ \boldsymbol{\mu}_{lk'}^H\boldsymbol{C}_{lk}\boldsymbol{\mu}_{lk'} + \boldsymbol{\mu}_{lk}^H\check{\boldsymbol{C}}_{lk'}\boldsymbol{\mu}_{lk} + \mathrm{trace}\left(\boldsymbol{T}_{lkk'}\right), \text{o/w}, \end{cases} \tag{23}$$

where

$$\boldsymbol{T}_{lkk'} = \boldsymbol{C}_{lk}\circ\check{\boldsymbol{C}}_{lk'} + \tau_{\mathrm{p}}\rho_{\mathrm{p}}\sigma_{\mathrm{p},l}^2\boldsymbol{C}_{lk}^{*}\boldsymbol{C}_{lk'}\boldsymbol{E}_{lk'}^{-1}(\boldsymbol{C}_{lk'}\boldsymbol{E}_{lk'}^{-1})^H, \tag{24}$$

$$\check{\boldsymbol{C}}_{lk'} = \tau_{\mathrm{p}}^2\rho_{\mathrm{p}}^2\boldsymbol{C}_{lk'}\boldsymbol{E}_{lk'}^{-1}\boldsymbol{C}_{lk'}\boldsymbol{E}_{lk'}^{-H}\boldsymbol{C}_{lk'}^H, \tag{25}$$

and $\boldsymbol{\mu}_{lk}$, $\boldsymbol{C}_{lk}$, $\boldsymbol{E}_{lk}$, $\hat{\boldsymbol{C}}_{lk}$, $\hat{\boldsymbol{R}}_{lk}$ and $\tilde{\boldsymbol{R}}_{lk}$ are given in (7)–(11). In (24), $\circ$ represents a Hadamard product.

Proof: See Appendix B. □

Based on Theorem 2, we derive the throughput of the considered system under independent and identically distributed (i.i.d.) Rayleigh fading channels in the following remark.

Remark 1: In the case that all the channels $\boldsymbol{h}_{lk}^{\mathrm{UA}}$, $\boldsymbol{h}_{km}^{\mathrm{US}}$, and $\boldsymbol{H}_{lm}^{\mathrm{SA}}$ follow i.i.d. Rayleigh fading model, $\mathcal{T}_k$ becomes $\mathcal{T}_k^{\mathrm{iid}}$ given in (26) (at the top of the next page), where $\gamma_{lk} \triangleq$

$$\mathcal{T}_k(\boldsymbol{\eta},\boldsymbol{\alpha}) = \frac{B_0\tau_{\mathrm{d}}}{\tau_{\mathrm{c}}}\log_2\left(1+\frac{\rho_{\mathrm{d}}\left|\boldsymbol{u}_k^T(\boldsymbol{\alpha})\bar{\boldsymbol{\eta}}_k\right|^2}{\rho_{\mathrm{d}}\sum_{k'\neq k}^{K}\left|\boldsymbol{v}_{kk'}^T(\boldsymbol{\alpha})\bar{\boldsymbol{\eta}}_{k'}\right|^2+\rho_{\mathrm{d}}\sum_{k'=1}^{K}\left\|\boldsymbol{D}_{kk'}(\boldsymbol{\alpha})\bar{\boldsymbol{\eta}}_{k'}\right\|^2+\sigma_{\mathrm{d},k}^2(\boldsymbol{\alpha})}\right) \tag{16}$$

$$\mathcal{T}_k^{\mathrm{iid}}(\boldsymbol{\eta},\boldsymbol{\alpha}) = \frac{B_0\tau_{\mathrm{d}}}{\tau_{\mathrm{c}}}\log_2\left(1+\frac{\rho_{\mathrm{d}}N_{\mathrm{A}}^2\left(\sum_{l=1}^{L}\eta_{lk}^{1/2}\gamma_{lk}\right)^2}{\rho_{\mathrm{d}}N_{\mathrm{A}}\sum_{k'=1}^{K}\sum_{l=1}^{L}\eta_{lk}\zeta_{lk}\gamma_{lk'}+\sigma_{\mathrm{d},k}^2(\boldsymbol{\alpha})}\right) \tag{26}$$

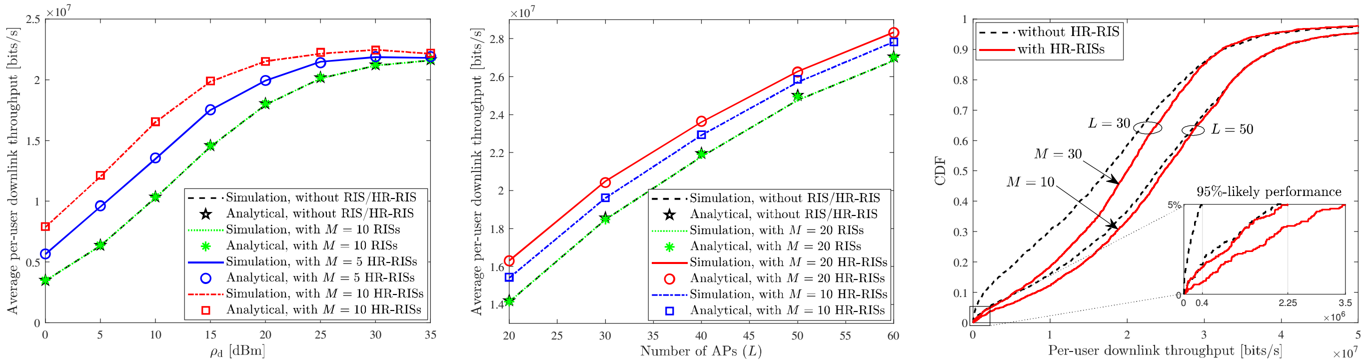

(a) Average $\mathcal{T}_k$ vs. ρ_{d} (b) Average $\mathcal{T}_k$ vs. L (c) CDF of $\mathcal{T}_k$

Fig. 2. Downlink per-user throughput of the HR-RIS-aided CF mMIMO systems with $N_{\mathrm{A}}=2$, $N=40$, $N_{\mathrm{R}}=1$, $\rho_{\mathrm{S,max}}=-3$ dBm, and (a) $L=30$, $M=\{5,10\}$, $K=5$; (b) $L\in[20,60]$, $M=\{10,20\}$, $K=10$, $\rho_{\mathrm{d}}=200$ mW; (c) $L=\{30,50\}$, $M=\{10,30\}$, $K=10$, $\rho_{\mathrm{d}}=200$ mW [1].

$\frac{\tau_{\mathrm{p}}\rho_{\mathrm{p}}\zeta_{lk}^2}{\tau_{\mathrm{p}}\rho_{\mathrm{p}}\zeta_{lk}+\sigma_{\mathrm{p},l}^2}$ with $\zeta_{lk}\triangleq\zeta_{lk}^{\mathrm{UA}}+\sum_{m=1}^{M}\sum_{n=1}^{N}|\alpha_{mn}|^2\zeta_{km}^{\mathrm{US}}\zeta_{lm}^{\mathrm{SA}}$. It is seen from (26) that, as $LN_{\mathrm{A}}\to\infty$, the received signal becomes free of interference and noise, like in the conventional CF mMIMO system [1].

We omit the proof of Remark 1 since (26) can be easily obtained by setting $\mu_{lkt}^{\mathrm{UA}}=\mu_{kmn}^{\mathrm{US}}=\mu_{lmnt}^{\mathrm{SA}}=0,\forall l,k,m,n,t$ for i.i.d. Rayleigh fading channels. We note that when $M=0$ (i.e., no HR-RIS is employed), (26) is in line with the result in [1]. This further confirms that the closed-from expression of the throughput is also valid for the conventional CF mMIMO system without RISs/HR-RISs. For the passive RIS-aided CF mMIMO system, the closed-from expression of the throughput can be derived by setting $|\alpha_{mn}|=1,\forall m,n$.

IV. Simulation Results

We provide numerical results to verify the analytical derivations. In the simulations, APs and UEs are randomly distributed over the entire coverage area of 1×1 km^2 [1], [19], while RISs/HR-RISs are randomly deployed inside circles of a radius of 10 m centred by the UEs, implying that RISs/HR-RISs are in the vicinity of the UEs. The large-scale fading coefficients $\zeta\in\{\zeta_{lk}^{\mathrm{UA}},\zeta_{km}^{\mathrm{US}},\zeta_{lm}^{\mathrm{SA}}\}$ are modeled based on the three-slope path loss model in [1], [19]. Rician factor $\kappa\in\{\kappa_{lk}^{\mathrm{UA}},\kappa_{km}^{\mathrm{US}},\kappa_{lm}^{\mathrm{SA}}\}$ for a distance d m is set to $\kappa=P_{\mathrm{LoS}}(d)/\left(1-P_{\mathrm{LoS}}(d)\right)$, where $P_{\mathrm{LoS}}(d)=\min\left(\frac{18}{d},1\right)\left(1-\exp(-\frac{d}{63})\right)+\exp(-\frac{d}{63})$ is the LoS probability [20], following the 3GPP–UMa model. The small scale fading channels are generated the same as in [3], [7] with details omitted due to limited space.

In the simulation, we adopt simple equal power control schemes to obtain power control coefficients $\{\eta_{lk}\}$, i.e., $\eta_{lk}=\left(\sum_{k'=1}^{K}\left(N_{\mathrm{A}}\gamma_{lk'}^{\mathrm{UA}}+\left\|\boldsymbol{\mu}_{lk'}^{\mathrm{UA}}\right\|^2\right)\right)^{-1},\forall l,k$ [1], [19]. The phases $\{\theta_{mn}\}$ are randomly generated, while $\{|\alpha_{mn}|\},n\in\mathcal{A}_m$ are generated based on exhaustive search such that the total transmit power of each HR-RIS is limited by a given power budget, denoted by $\rho_{\mathrm{S,max}}$, and equally shared among the active elements. The positions of active elements of HR-RISs are randomly generated. The noise power is given as $\sigma_{\mathrm{N}}^2=-170+10\log_{10}(B_0)+\mathrm{NF}$ (dBm), where $B_0=20$ MHz and noise figure $\mathrm{NF}=9$ dB. We set the normalized residual SI power to 1 dB [16], $\tau_{\mathrm{p}}=K$, $\tau_{\mathrm{c}}=200$, and $\rho_{\mathrm{p}}=100$ mW [1], [21]. The other simulation parameters are listed in the caption of Fig. 2. For comparisons, we consider the conventional CF mMIMO systems without any HR-RIS and that with passive RISs. Note that each HR-RIS requires an additional power budget $\rho_{\mathrm{S,max}}$. Therefore, for fair comparisons, the transmit power at each AP in the HR-RIS-aided CF mMIMO system is reduced by an amount of $\frac{M\rho_{\mathrm{S,max}}}{L}$ so that all the compared schemes have the same total transmit power.

Fig. 2(a) shows the downlink throughput obtained by analytical derivations and those obtained by Monte Carlo simulations for various values of ρ_{d}. It is observed that the theoretical analysis results align well with the simulation ones in the entire considered range of ρ_{d}, validating the derivations in Theorem 2. Furthermore, it is clear that with random phase shifts, passive RISs offer negligible performance gain for CF mMIMO systems. In contrast, HR-RISs provide considerable throughput improvement, and the gain is more significant at low and moderate ρ_{d} thanks to its capability of amplifying the incident signals. Furthermore, it is clear that a larger M leads to a more significant improvement.

In Fig. 2(b), we investigate the significance of HR-RISs for systems with different numbers of APs, i.e., $L\in[20,60]$. As seen, the theoretical analytical results still align well with the simulation ones. While the performance improvement of the passive RISs is still negligible, HR-RISs offer a considerable improvement in throughput even when L is large. However, it is observed that the improvement is slightly degraded as L increases, which is reasonable because when there are more APs, HR-RISs become less important.

Finally, to highlight the advantage of the HR-RISs, we plot the cumulative distributions (CDFs) of the per-user downlink throughput in Fig. 2(c). It shows that the system assisted by HR-RISs outperforms the conventional one in both median and 95%-likely performance. Specifically, with $L = 30$, the 95%-likely per-user downlink throughput of the conventional CF mMIMO system without HR-RIS is only 0.4 Mbits/s, while that of the proposed HR-RIS-aided system is 2.25 Mbits/s, implying 5.6 times improvement. The corresponding improvement for $L = 50$ is less significant (1.75 times).

V. Conclusion

This work has considered the novel HR-RIS-aided CF mMIMO system in which HR-RISs are equipped with both active relay and passive reflecting elements to assist communications between multiple APs and UEs. We have derived the MMSE estimate of the effective channels and provided closed-form expressions for the downlink throughput of the system under the Rician fading channel model. The analytical derivations have been numerically justified by simulations, showing that the proposed system achieves significant performance improvement in terms of per-user throughput, especially when the transmit power of APs is low and/or when the number of APs is large enough.

Acknowledgment

This work has been supported in part by Academy of Finland under 6Genesis Flagship (grant 318927), EERA Project (grant 332362), and Infotech Program funded by University of Oulu Graduate School.

Appendix A
Proof of Theorem 1

The MMSE estimate of $\boldsymbol{g}_{lk}$ is computed as

$$\hat{\boldsymbol{g}}_{lk} = \mathbb{E}\{\boldsymbol{g}_{lk}\} + \mathbb{C}\{\boldsymbol{g}_{lk}, \boldsymbol{y}_{lk}\}\,\mathbb{C}\{\boldsymbol{y}_{lk}\}^{-1}\left(\boldsymbol{y}_{lk} - \mathbb{E}\{\boldsymbol{y}_{lk}\}\right). \quad (27)$$

First, from (1), we have

$$\mathbb{E}\{\boldsymbol{g}_{lk}\} = \boldsymbol{\mu}_{lk}^{\mathrm{UA}} + \sum_{m=1}^{M}\sum_{n=1}^{N} \alpha_{mn}\bar{\boldsymbol{\mu}}_{lkmn}^{\mathrm{USA}} \triangleq \boldsymbol{\mu}_{lk}, \quad (28)$$

where $\bar{\boldsymbol{\mu}}_{lkmn}^{\mathrm{USA}} \triangleq \boldsymbol{\mu}_{lmn}^{\mathrm{SA}}\mu_{kmn}^{\mathrm{US}}$. Noting that $\mathbb{E}\{\tilde{\boldsymbol{z}}_{lk}\} = \boldsymbol{0}$ and from (5), we obtain

$$\mathbb{E}\{\boldsymbol{y}_{lk}\} = \mathbb{E}\left\{\sqrt{\tau_{\mathrm{p}}\rho_{\mathrm{p}}}\boldsymbol{g}_{lk} + \tilde{\boldsymbol{z}}_{lk}\right\} = \sqrt{\tau_{\mathrm{p}}\rho_{\mathrm{p}}}\boldsymbol{\mu}_{lk}. \quad (29)$$

By using $\boldsymbol{y}_{lk} = \sqrt{\tau_{\mathrm{p}}\rho_{\mathrm{p}}}\boldsymbol{g}_{lk} + \tilde{\boldsymbol{z}}_{lk}$, $\mathbb{C}\{\boldsymbol{g}_{lk}, \boldsymbol{y}_{lk}\}$ is computed as

$$\mathbb{C}\{\boldsymbol{g}_{lk}, \boldsymbol{y}_{lk}\} = \sqrt{\tau_{\mathrm{p}}\rho_{\mathrm{p}}}\mathbb{C}\{\boldsymbol{g}_{lk}\} + \mathbb{C}\{\boldsymbol{g}_{lk}, \tilde{\boldsymbol{z}}_{lk}\} \overset{(a)}{=} \sqrt{\tau_{\mathrm{p}}\rho_{\mathrm{p}}}\boldsymbol{C}_{lk}. \quad (30)$$

Here, $\boldsymbol{C}_{lk} \triangleq \mathbb{C}\{\boldsymbol{g}_{lk}\}$, and equality (a) can be obtained by expanding $\mathbb{C}\{\boldsymbol{g}_{lk}, \tilde{\boldsymbol{z}}_{lk}\} = \mathbb{E}\left\{\boldsymbol{g}_{lk}\tilde{\boldsymbol{z}}_{lk}^H\right\} - \mathbb{E}\{\boldsymbol{g}_{lk}\}\mathbb{E}\{\tilde{\boldsymbol{z}}_{lk}\}^H = \boldsymbol{0}_{N_{\mathrm{A}}}$ due to $\mathbb{E}\left\{\boldsymbol{g}_{lk}\tilde{\boldsymbol{z}}_{lk}^H\right\} = \boldsymbol{0}_{N_{\mathrm{A}}}$ and $\mathbb{E}\{\tilde{\boldsymbol{z}}_{lk}\} = \boldsymbol{0}$ as the noise entries/elements of $\boldsymbol{Z}_{\mathrm{A},l}$, $z_{\mathrm{SI},mn}$ and $z_{\mathrm{N},mn}$ are independent of $\boldsymbol{g}_{lk}$ and have zero means $\forall l, m, n$. Furthermore, $\boldsymbol{C}_{lk}$ can be computed based on (1), as $\boldsymbol{C}_{lk} = \mathbb{C}\{\boldsymbol{g}_{lk}\} = \mathbb{C}\left\{\boldsymbol{h}_{lk}^{\mathrm{UA}}\right\} + \sum_{m=1}^{M}\sum_{n=1}^{N}|\alpha_{mn}|^2\,\mathbb{C}\left\{\boldsymbol{h}_{lmn}^{\mathrm{SA}}h_{kmn}^{\mathrm{US}}\right\}$. Here, $\mathbb{C}\left\{\boldsymbol{h}_{lk}^{\mathrm{UA}}\right\} = \beta_{lk}^{\mathrm{UA}}\mathbf{I}_{N_{\mathrm{A}}}$, and $\mathbb{C}\left\{\boldsymbol{h}_{lmn}^{\mathrm{SA}}h_{kmn}^{\mathrm{US}}\right\} = \bar{\boldsymbol{\mathcal{B}}}_{lkmn}^{\mathrm{USA}}$ defined in Theorem 1, which is obtained based on the independence between $\boldsymbol{h}_{lmn}^{\mathrm{SA}}$ and h_{kmn}^{US} and the fact that $\mathbb{E}\left\{\boldsymbol{h}_{lmn}^{\mathrm{SA}}(\boldsymbol{h}_{lmn}^{\mathrm{SA}})^H\right\} = \beta_{lm}^{\mathrm{SA}}\mathbf{I}_{N_{\mathrm{A}}} + \boldsymbol{\mu}_{lmn}^{\mathrm{SA}}\left(\boldsymbol{\mu}_{lmn}^{\mathrm{SA}}\right)^H$. Furthermore, $\mathbb{C}\{\boldsymbol{y}_{lk}\}$ can be computed based on (5) as

$$\mathbb{C}\{\boldsymbol{y}_{lk}\} = \mathbb{C}\left\{\sqrt{\tau_{\mathrm{p}}\rho_{\mathrm{p}}}\boldsymbol{g}_{lk} + \tilde{\boldsymbol{z}}_{lk}\right\} = \boldsymbol{E}_{lk}, \quad (31)$$

where $\boldsymbol{E}_{lk}$ is defined in Theorem 1.

Finally, by substituting (28)–(31) into (27), we obtain (6). We have $\mathbb{E}\{\hat{\boldsymbol{g}}_{lk}\} = \boldsymbol{\mu}_{lk}$ from (27), and $\mathbb{C}\{\hat{\boldsymbol{g}}_{lk}\} = \tau_{\mathrm{p}}\rho_{\mathrm{p}}\boldsymbol{C}_{lk}\boldsymbol{E}_{lk}^{-1}\mathbb{C}\{\boldsymbol{y}_{lk}\}\left(\boldsymbol{C}_{lk}\boldsymbol{E}_{lk}^{-1}\right)^H = \hat{\boldsymbol{C}}_{lk}$ from (31). Besides, by using $\mathbb{C}\{\hat{\boldsymbol{g}}_{lk}\} = \mathbb{E}\left\{\hat{\boldsymbol{g}}_{lk}\hat{\boldsymbol{g}}_{lk}^H\right\} - \mathbb{E}\{\hat{\boldsymbol{g}}_{lk}\}\mathbb{E}\{\hat{\boldsymbol{g}}_{lk}\}^H$, $\mathbb{E}\left\{\hat{\boldsymbol{g}}_{lk}\hat{\boldsymbol{g}}_{lk}^H\right\}$ and $\mathbb{E}\left\{\|\hat{\boldsymbol{g}}_{lk}\|^2\right\}$ are obtained as in (9) and (10), respectively. The estimation error is given by $\tilde{\boldsymbol{g}}_{lk} = \boldsymbol{g}_{lk} - \hat{\boldsymbol{g}}_{lk}$. Because $\mathbb{E}\{\boldsymbol{g}_{lk}\} = \mathbb{E}\{\hat{\boldsymbol{g}}_{lk}\} = \boldsymbol{\mu}_{lk}$, it is clear that $\mathbb{E}\{\tilde{\boldsymbol{g}}_{lk}\} = \boldsymbol{0}$, and thus, $\mathbb{C}\{\tilde{\boldsymbol{g}}_{lk}\} = \mathbb{E}\left\{\tilde{\boldsymbol{g}}_{lk}\tilde{\boldsymbol{g}}_{lk}^H\right\} = \boldsymbol{C}_{lk} - \hat{\boldsymbol{C}}_{lk} \triangleq \tilde{\boldsymbol{R}}_{lk}$.

Appendix B
Proof of Theorem 2

- *Compute* $|\mathrm{DS}_k|^2$*:* Because $\boldsymbol{g}_{lk} = \tilde{\boldsymbol{g}}_{lk} + \hat{\boldsymbol{g}}_{lk}$ and $\tilde{\boldsymbol{g}}_{lk}$ and $\hat{\boldsymbol{g}}_{lk}$ are uncorrelated, we have $\mathrm{DS}_k = \sqrt{\rho_{\mathrm{d}}}\sum_{l=1}^{L}\sqrt{\eta_{lk}}\left(\mathbb{E}\left\{\tilde{\boldsymbol{g}}_{lk}^T\hat{\boldsymbol{g}}_{lk}^*\right\} + \mathbb{E}\left\{\|\hat{\boldsymbol{g}}_{lk}\|^2\right\}\right)$. By using the result in (10) and definitions (18), (21), we obtain

$$|\mathrm{DS}_k|^2 = \sqrt{\rho_{\mathrm{d}}}\sum_{l=1}^{L}\sqrt{\eta_{lk}}u_{lk}(\boldsymbol{\alpha}) = \rho_{\mathrm{d}}\left|\boldsymbol{u}_k(\boldsymbol{\alpha})^T\bar{\boldsymbol{\eta}}_k\right|^2. \quad (32)$$

- *Compute* $\mathbb{E}\left\{|\mathrm{BU}_k|^2\right\}$*:* We rewrite BU_k as $\mathrm{BU}_k = \sqrt{\rho_{\mathrm{d}}}\sum_{l=1}^{L}\sqrt{\eta_{lk}}q_{lk}$, where $q_{lk} \triangleq \boldsymbol{g}_{lk}^T\hat{\boldsymbol{g}}_{lk}^* - \mathbb{E}\left\{\boldsymbol{g}_{lk}^T\hat{\boldsymbol{g}}_{lk}^*\right\}$. Thus,

$$\mathbb{E}\left\{|\mathrm{BU}_k|^2\right\} = \rho_{\mathrm{d}}\sum_{l=1}^{L}\eta_{lk}\mathbb{E}\left\{|q_{lk}|^2\right\} + \rho_{\mathrm{d}}\sum_{l=1}^{L}\sum_{l'\neq l}^{L}\sqrt{\eta_{lk}\eta_{l'k}}\left(\mathbb{E}\left\{q_{lk}q_{l'k}^*\right\} + \mathbb{E}\left\{q_{lk}^*q_{l'k}\right\}\right).$$

Here, using $\boldsymbol{g}_{lk} = \tilde{\boldsymbol{g}}_{lk} + \hat{\boldsymbol{g}}_{lk}$, we can write $\mathbb{E}\left\{q_{lk}q_{l'k}^*\right\} = \mathbb{E}\left\{\|\hat{\boldsymbol{g}}_{lk}\|^2\|\hat{\boldsymbol{g}}_{l'k}\|^2\right\} - \mathbb{E}\left\{\|\hat{\boldsymbol{g}}_{lk}\|^2\right\}\mathbb{E}\left\{\|\hat{\boldsymbol{g}}_{l'k}\|^2\right\}$, which represents the correlation between $\hat{\boldsymbol{g}}_{lk}$ and $\hat{\boldsymbol{g}}_{l'k}$. Based on (1), (5), and (6), we can write $\hat{\boldsymbol{g}}_{lk} = \boldsymbol{\mu}_{lk} + \sqrt{\tau_{\mathrm{p}}\rho_{\mathrm{p}}}\boldsymbol{C}_{lk}\boldsymbol{E}_{lk}^{-1}\left(\sqrt{\tau_{\mathrm{p}}\rho_{\mathrm{p}}}\tilde{\boldsymbol{h}}_{lk} + \tilde{\boldsymbol{z}}_{lk}\right)$, where

$$\tilde{\boldsymbol{h}}_{lk} \triangleq \sqrt{\beta_{lk}^{\mathrm{UA}}}\tilde{\boldsymbol{h}}_{lk}^{\mathrm{UA}} + \sum_{m=1}^{M}\sum_{n=1}^{N}\alpha_{mn}\left(\mu_{kmn}^{\mathrm{US}}\sqrt{\beta_{lm}^{\mathrm{SA}}}\tilde{\boldsymbol{h}}_{lmn}^{\mathrm{SA}} + \boldsymbol{\mu}_{lmn}^{\mathrm{SA}}\sqrt{\beta_{km}^{\mathrm{US}}}\tilde{h}_{kmn}^{\mathrm{US}} + \sqrt{\beta_{lm}^{\mathrm{SA}}}\tilde{\boldsymbol{h}}_{lmn}^{\mathrm{SA}}\sqrt{\beta_{km}^{\mathrm{US}}}\tilde{h}_{kmn}^{\mathrm{US}}\right).$$

It is observed that $\hat{\boldsymbol{g}}_{lk}$ and $\hat{\boldsymbol{g}}_{l'k}$ are correlated due to the common coefficient $\tilde{h}_{kmn}^{\mathrm{US}}$ in the last two terms of $\tilde{\boldsymbol{h}}_{lk}$. However, when HR-RISs are placed in the vicinity of either UEs or APs to improve the system performance, these terms are very small compared to the overall channel coefficients of $\hat{\boldsymbol{g}}_{lk}$ and $\hat{\boldsymbol{g}}_{l'k}$. Specifically, when the mth HR-RIS is near the kth UE, the LoS links between the HR-RIS and the UE is strong, but that between the AP and the HR-RIS is weak and the path loss is large, leading to $\sqrt{\beta_{lm}^{\mathrm{SA}}}\tilde{\boldsymbol{h}}_{lmn}^{\mathrm{SA}} \approx \boldsymbol{0}$ and $\boldsymbol{\mu}_{lmn}^{\mathrm{SA}} \approx \boldsymbol{0}$. Similarly, we have $\sqrt{\beta_{km}^{\mathrm{US}}}\tilde{h}_{kmn}^{\mathrm{US}} \approx 0$ for the latter case. Therefore, in both cases, the correlation between $\hat{\boldsymbol{g}}_{lk}$ and $\hat{\boldsymbol{g}}_{l'k}$ can be negligible, and thus $\mathbb{E}\{q_{lk}q_{l'k}^*\} + \mathbb{E}\{q_{lk}^* q_{l'k}\} \approx 0$. This leads to

$$\mathbb{E}\left\{|\mathrm{BU}_k|^2\right\} \approx \rho_{\mathrm{d}} \sum_{l=1}^{L} \eta_{lk} \left|\left(\boldsymbol{g}_{lk}^H \hat{\boldsymbol{g}}_{lk} - \mathbb{E}\left\{\boldsymbol{g}_{lk}^H \hat{\boldsymbol{g}}_{lk}\right\}\right)\right|^2$$
$$= \rho_{\mathrm{d}} \sum_{l=1}^{L} \eta_{lk} \left(\mathbb{E}\left\{\|\hat{\boldsymbol{g}}_{lk}\|^4\right\} + \mathbb{E}\left\{\left|\tilde{\boldsymbol{g}}_{lk}^H \hat{\boldsymbol{g}}_{lk}\right|^2\right\} - \left(\mathrm{trace}\left(\hat{\boldsymbol{C}}_{lk}\right) + \|\boldsymbol{\mu}_{lk}\|^2\right)^2\right). \quad (33)$$

We note that $\boldsymbol{g}_{lk}$ is given in (1) as the sum of $MN+1$ vectors, where MN is equal to the total number of elements of all HR-RISs and is very large. Therefore, the distributions of $\boldsymbol{g}_{lk}$ and $\hat{\boldsymbol{g}}_{lk}$ can be approximated as $\mathcal{CN}(\boldsymbol{\mu}_{lk}, \boldsymbol{C}_{lk})$ and $\mathcal{CN}(\boldsymbol{\mu}_{lk}, \hat{\boldsymbol{C}}_{lk})$, respectively. By using [22, Lemma 9], we have

$$\mathbb{E}\left\{\|\hat{\boldsymbol{g}}_{lk}\|^4\right\} = \|\boldsymbol{\mu}_{lk}\|^4 + 2\|\boldsymbol{\mu}_{lk}\|^2 \mathrm{trace}\left(\hat{\boldsymbol{C}}_{lk}\right) + 2\boldsymbol{\mu}_{lk}^H \hat{\boldsymbol{C}}_{lk} \boldsymbol{\mu}_{lk} + \left|\mathrm{trace}\left(\hat{\boldsymbol{C}}_{lk}\right)\right|^2 + \mathrm{trace}\left(\hat{\boldsymbol{C}}_{lk}^2\right). \quad (34)$$

Since $\tilde{\boldsymbol{g}}_{lk}$ and $\hat{\boldsymbol{g}}_{lk}$ are uncorrelated and $\mathbb{E}\{\tilde{\boldsymbol{g}}_{lk}\} = \boldsymbol{0}$, we obtain

$$\mathbb{E}\left\{\left|\tilde{\boldsymbol{g}}_{lk}^H \hat{\boldsymbol{g}}_{lk}\right|^2\right\} = \mathrm{trace}\left(\tilde{\boldsymbol{R}}_{lk} \circ \hat{\boldsymbol{R}}_{lk}\right). \quad (35)$$

From (33)–(35), and the definitions (20), (23) we obtain

$$\mathbb{E}\left\{|\mathrm{BU}_k|^2\right\} \approx \rho_{\mathrm{d}} \sum_{l=1}^{L} \eta_{lk} d_{lkk}(\boldsymbol{\alpha}) = \rho_{\mathrm{d}} \|\boldsymbol{D}_{kk}(\boldsymbol{\alpha})\boldsymbol{\omega}_k\|^2. \quad (36)$$

• *Compute* $\mathbb{E}\left\{|\mathrm{UI}_{kk'}|^2\right\}$*:* First, $\hat{\boldsymbol{g}}_{lk'}$ in (6) can be rewritten as $\hat{\boldsymbol{g}}_{lk'} = \check{\boldsymbol{g}}_{lk'} + \sqrt{\tau_{\mathrm{p}}\rho_{\mathrm{p}}}\boldsymbol{C}_{lk'}\boldsymbol{E}_{lk'}^{-1}\tilde{\boldsymbol{z}}_{lk'}$, where $\check{\boldsymbol{g}}_{lk'} \triangleq \left(\mathbf{I}_{N_{\mathrm{A}}} - \tau_{\mathrm{p}}\rho_{\mathrm{p}}\boldsymbol{C}_{lk'}\boldsymbol{E}_{lk'}^{-1}\right)\boldsymbol{\mu}_{lk'} + \tau_{\mathrm{p}}\rho_{\mathrm{p}}\boldsymbol{C}_{lk'}\boldsymbol{E}_{lk'}^{-1}\boldsymbol{g}_{lk'}$. As a result, we obtain $\mathbb{E}\left\{|\mathrm{UI}_{kk'}|^2\right\} = \rho_{\mathrm{d}}(\mathcal{J}_1 + \mathcal{J}_2 + \mathcal{J}_3)$, where $\mathcal{J}_1 \triangleq \mathbb{V}\mathrm{ar}\left(\sum_{l=1}^{L}\sqrt{\eta_{lk'}}\boldsymbol{g}_{lk}^T\check{\boldsymbol{g}}_{lk'}^*\right)$, $\mathcal{J}_2 \triangleq \left|\mathbb{E}\left\{\sum_{l=1}^{L}\sqrt{\eta_{lk'}}\boldsymbol{g}_{lk}^T\check{\boldsymbol{g}}_{lk'}^*\right\}\right|^2$, and $\mathcal{J}_3 \triangleq \mathbb{E}\left\{\sum_{l=1}^{L}\left|\sqrt{\eta_{lk'}}\sqrt{\tau_{\mathrm{p}}\rho_{\mathrm{p}}}\boldsymbol{g}_{lk}^T\boldsymbol{C}_{lk'}\boldsymbol{E}_{lk'}^{-1}\tilde{\boldsymbol{z}}_{lk'}^*\right|^2\right\}$. By a similar analysis as for $\mathbb{E}\left\{|\mathrm{BU}_k|^2\right\}$, the correlation between $\boldsymbol{g}_{lk}$ and $\check{\boldsymbol{g}}_{lk'}$ in $\mathcal{J}_1$ and $\mathcal{J}_2$ and that between $\boldsymbol{g}_{lk}$ and $\tilde{\boldsymbol{z}}_{lk'}$ in $\mathcal{J}_3$ can be neglected. Then, $\mathcal{J}_1$, $\mathcal{J}_2$, and $\mathcal{J}_3$ are approximated as

$$\mathcal{J}_1 \approx \sum_{l=1}^{L}\eta_{lk'}\sum_{t=1}^{N_{\mathrm{A}}}\mathbb{V}\mathrm{ar}\left(g_{lkt}\check{g}_{lk't}^*\right) = \sum_{l=1}^{L}\eta_{lk'}\mathrm{trace}\left(\boldsymbol{C}_{lk}\circ\check{\boldsymbol{C}}_{lk'} + \boldsymbol{C}_{lk}\boldsymbol{\mu}_{lk'}\boldsymbol{\mu}_{lk'}^H + \check{\boldsymbol{C}}_{lk'}\boldsymbol{\mu}_{lk}\boldsymbol{\mu}_{lk}^H\right), \quad (37)$$

$$\mathcal{J}_2 \approx \left|\sum_{l=1}^{L}\sqrt{\eta_{lk'}}\boldsymbol{\mu}_{lk}^T\boldsymbol{\mu}_{lk'}^*\right|^2 = \left|\boldsymbol{v}_{kk'}^T(\boldsymbol{\alpha})\bar{\boldsymbol{\eta}}_{k'}\right|^2, \quad (38)$$

$$\mathcal{J}_3 \approx \sum_{l=1}^{L}\eta_{lk'}\tau_{\mathrm{p}}\rho_{\mathrm{p}}\mathbb{E}\left\{\left|\boldsymbol{g}_{lk}^T\boldsymbol{C}_{lk'}\boldsymbol{E}_{lk'}^{-1}\tilde{\boldsymbol{z}}_{lk'}^*\right|^2\right\} = \sum_{l=1}^{L}\eta_{lk'}\tau_{\mathrm{p}}\rho_{\mathrm{p}}\sigma_{\mathrm{p},l}^2 \times \mathrm{trace}\left(\left(\boldsymbol{C}_{lk} + \boldsymbol{\mu}_{lk}\boldsymbol{\mu}_{lk}^H\right)\boldsymbol{C}_{lk'}\boldsymbol{E}_{lk'}^{-1}(\boldsymbol{C}_{lk'}\boldsymbol{E}_{lk'}^{-1})^H\right) \quad (39)$$

where $v_{lkk'}(\boldsymbol{\alpha})$ and $\boldsymbol{v}_{kk'}(\boldsymbol{\alpha})$ in (38) are defined in (19), (22). As a result, $\mathbb{E}\left\{|\mathrm{UI}_{kk'}|^2\right\}$ can be written as

$$\mathbb{E}\left\{|\mathrm{UI}_{kk'}|^2\right\} \approx \rho_{\mathrm{d}}\left|\boldsymbol{v}_{kk'}^T(\boldsymbol{\alpha})\bar{\boldsymbol{\eta}}_{k'}\right|^2 + \rho_{\mathrm{d}}\sum_{l=1}^{L}\eta_{lk'}\mathrm{trace}\left(\bar{\boldsymbol{C}}_{lkk'}\right)$$
$$= \rho_{\mathrm{d}}\left|\boldsymbol{v}_{kk'}^T(\boldsymbol{\alpha})\bar{\boldsymbol{\eta}}_{k'}\right|^2 + \rho_{\mathrm{d}}\left\|\boldsymbol{D}_{kk'}(\boldsymbol{\alpha})\bar{\boldsymbol{\eta}}_{k'}\right\|^2, \quad (40)$$

where $\bar{\boldsymbol{C}}_{lkk'} \triangleq \boldsymbol{C}_{lk}\boldsymbol{\mu}_{lk'}\boldsymbol{\mu}_{lk'}^H + \check{\boldsymbol{C}}_{lk'}\boldsymbol{\mu}_{lk}\boldsymbol{\mu}_{lk}^H + \mathrm{trace}\left(\boldsymbol{T}_{lkk'}\right)$ with $\boldsymbol{T}_{lkk'}$ and $\boldsymbol{D}_{kk'}(\boldsymbol{\alpha})$ given in (24) and (20), respectively.

Finally, by substituting the results in (32), (36) and (40) into (15), we obtain (16) which completes the proof.

References

[1] H. Q. Ngo, A. Ashikhmin, H. Yang, E. G. Larsson, and T. L. Marzetta, "Cell-free massive MIMO versus small cells," *IEEE Trans. Wireless Commun.*, vol. 16, no. 3, pp. 1834–1850, 2017.

[2] N. T. Nguyen, Q.-D. Vu, K. Lee, and M. Juntti, "Spectral efficiency optimization for hybrid relay-reflecting intelligent surface," *IEEE Int. Conf. Commun. Workshops (ICCW)*, 2021.

[3] ——, "Hybrid relay-reflecting intelligent surface-assisted wireless communication," *arXiv preprint arXiv:2103.03900*, 2021.

[4] N. T. Nguyen *et al.*, "Hybrid relay-reflecting intelligent surface-aided wireless communications: Opportunities, challenges, and future perspectives," *arXiv preprint arXiv:2104.02039*, 2021.

[5] Y. Yang, B. Zheng, S. Zhang, and R. Zhang, "Intelligent reflecting surface meets OFDM: Protocol design and rate maximization," *IEEE Trans. Commun.*, 2020.

[6] Q. Wu and R. Zhang, "Intelligent reflecting surface enhanced wireless network via joint active and passive beamforming," *IEEE Trans. Wireless Commun.*, vol. 18, no. 11, pp. 5394–5409, 2019.

[7] S. Zhang and R. Zhang, "Capacity characterization for intelligent reflecting surface aided MIMO communication," *IEEE J. Sel. Areas Commun.*, vol. 38, no. 8, pp. 1823–1838, 2020.

[8] K. Ying *et al.*, "GMD-based hybrid beamforming for large reconfigurable intelligent surface assisted millimeter-wave massive MIMO," *IEEE Access*, vol. 8, pp. 19 530–19 539, 2020.

[9] N. T. Nguyen, L. V. Nguyen, T. Huynh-The, D. H. N. Nguyen, A. Lee Swindlehurst, and M. Juntti, "Machine learning-based reconfigurable intelligent surface-aided MIMO systems," in *IEEE Int. Work. Signal Process. Advances Wireless Commun. (SPAWC)*, 2021, pp. 101–105.

[10] Y. Zhang, B. Di, H. Zhang, J. Lin, Y. Li, and L. Song, "Reconfigurable intelligent surface aided cell-free MIMO communications," *IEEE Wireless Commun. Lett.*, 2020.

[11] Y. Zhang *et al.*, "Beyond cell-free MIMO: Energy efficient reconfigurable intelligent surface aided cell-free MIMO communications," *IEEE Trans. Cognitive Commun. Network.*, 2021.

[12] S. Huang, Y. Ye, M. Xiao, H. V. Poor, and M. Skoglund, "Decentralized beamforming design for intelligent reflecting surface-enhanced cell-free networks," *IEEE Wireless Commun. Lett.*, 2020.

[13] T. Van Chien *et al.*, "Reconfigurable intelligent surface-assisted cell-free massive MIMO systems over spatially-correlated channels," *arXiv preprint arXiv:2104.08648*, 2021.

[14] T. Zhou, K. Xu, X. Xia, W. Xie, and X. Yang, "Achievable rate maximization for aerial intelligent reflecting surface-aided cell-free massive MIMO system," in *IEEE ICCC*, 2020, pp. 623–628.

[15] K.-H. Ngo *et al.*, "Low-latency and secure computation offloading assisted by hybrid relay-reflecting intelligent surface," *arXiv preprint arXiv:2109.01335*, 2021.

[16] R. Malik and M. Vu, "Optimal transmission using a self-sustained relay in a full-duplex MIMO system," *IEEE J. Sel. Areas Commun.*, vol. 37, no. 2, pp. 374–390, 2018.

[17] Q. Wu, S. Zhang, B. Zheng, C. You, and R. Zhang, "Intelligent reflecting surface aided wireless communications: A tutorial," *IEEE Trans. Commun.*, vol. 69, no. 5, pp. 3313–3351, Jan. 2021.

[18] W. Tang *et al.*, "On channel reciprocity in reconfigurable intelligent surface assisted wireless network," *arXiv preprint arXiv:2103.03753*, 2021.

[19] H. Q. Ngo, L.-N. Tran, T. Q. Duong, M. Matthaiou, and E. G. Larsson, "On the total energy efficiency of cell-free massive MIMO," *IEEE Trans. Green Commun. Network.*, vol. 2, no. 1, pp. 25–39, 2017.

[20] I. Rodriguez *et al.*, "Path loss validation for urban micro cell scenarios at 3.5 GHz compared to 1.9 GHz," in *IEEE Global Commun. Conf. (GLOBECOM)*, 2013, pp. 3942–3947.

[21] D. Bharadia and S. Katti, "Full duplex MIMO radios," in *11th USENIX Symp. Netw. Syst. Design Implement. (NSDI)*, 2014, pp. 359–372.

[22] T. Van Chien and H. Q. Ngo, "Massive MIMO channels," *Antennas and Propagation for 5G and Beyond*, p. 301, 2020.